Dynamic Behavior of Active Lightweight Compliant Mechanisms with Integrated Piezoceramic Actuators by Under- and Overcritical Periodic Excitation

N. Modler, A. Winkler, A. Filippatos, Erwin-Christian Lovasz and D.-T. Mărgineanu

Abstract Integration of active elements as thermoplastic-compatible piezoceramic modules in lightweight compliant mechanisms offers the possibility to actively control its structural behavior by static, dynamic or vibro-acoustic loads. New active lightweight structures with material-integrated structural monitoring, energy-harvesting, or active vibration damping functionalities become possible. Previously, a demonstrator mechanism was designed and built, and its behavior under quasi-static excitation was simulated as a multi-body system, using two-layer cells with torsion and traction springs for compliance and linear motors for excitation. The mechanism was later tested to confirm the simulation results. This paper presents a study of the dynamic behavior of active compliant mechanisms obtained by integration of piezoceramic actuators into fiber-reinforced composite structures. The results of the dynamic mechanical simulation procedure were compared with experimental results for a given demonstrator mechanism. The comparison concluded that the simulation procedure describes fairly accurate the real behavior of the lightweight compliant mechanism, thus it can be used in the development of new active structures.

Keywords Compliant mechanisms · Piezoactuation · Dynamics · Oscillation

N. Modler · A. Winkler · A. Filippatos
Institute of Lightweight Engineering and Polymer Technology,
Technische Universität Dresden, Dresden, Germany
e-mail: niels.modler@ilk.mw.tu-dresden.de

A. Winkler
e-mail: anja.winkler@ilk.mw.tu-dresden.de

A. Filippatos
e-mail: angelos.filippatos@ilk.mw.tu-dresden.de

E.-C. Lovasz · D.-T. Mărgineanu (✉)
Department of Mechatronics, University Politehnica Timişoara,
Timişoara, Romania
e-mail: dan.margineanu@upt.ro

E.-C. Lovasz
e-mail: erwin.lovasz@upt.ro

213

1   Introduction

Compliant mechanisms, consisting of links with higher rigidity and/or with higher elasticity (compliant elements), revolute joints in hybrid structures or elastic joints in monolithic structures, can fulfill specified functions with a minimum number of elements and joints. Active compliant mechanisms (ACM) integrate sensors and actuators in the composite structure, further reducing complexity and costs. ACM movements depend both on rigid and elastic elements geometry and on load types which are influenced by elastic and inertial material properties (Modler 2008). Thus desired functions may be obtained only after consequently testing, re-design and adjustments, with resulting high time and cost effects.

A compliance comparison between multi-spring model and finite-element analysis was done (Gao 2010) for multidimensional accelerometers based on a fully decoupled compliant parallel mechanism. An under-actuated compliant variable stroke mechanism is analyzed (Tanık 2010) which employed Pseudo Rigid Body Model (PRBM) for prescribed output loading and constant input torque.

The development of FEM models requires dimensions, physical properties of used materials, etc. thus some dimensioning steps are previously required. Simulation models using cells composed of rigid links, revolute and prismatic joints, torsion and traction spring-dampers and linear actuators were presented in previous investigations (Modler 2009) as they were used for dynamic analysis of compliant mechanisms. The double layer model (Mărgineanu 2014) proved to be the most successful, as it has both compliance and actuation and the simulation parameters, e.g. the springs' rigidity and damping coefficients may be calculated according to the material properties and elements' dimensions. In this paper, the double layer model is used for dynamic analysis of a piezoelectric driven ACM by under- and overcritical periodic excitation.

2   Investigated Structure

The investigated mechanism presented in Fig. 1 under kinematic scheme is composed of an output link B_0B (4) connected to the frame (1) through the revolute joint B_0, with a counterweight for equilibration. The actuator A_0A (2) is rigidly

Fig. 1 Kinematic scheme of the active compliant mechanism
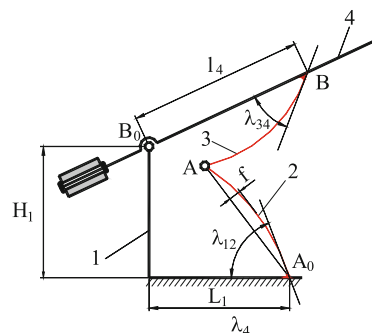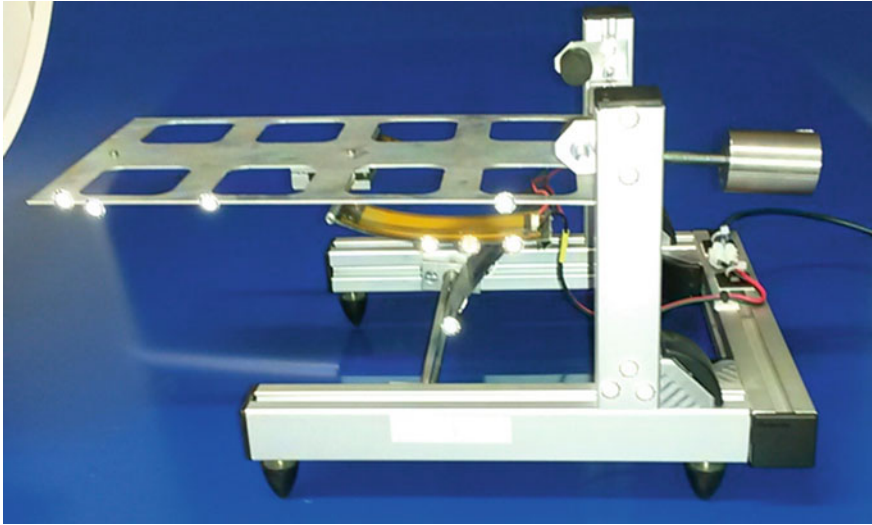
Fig. 2 The flap mechanism with two bending actuators demonstrator in the starting position

connected to the frame in A_0 at an adjustable angle λ_{12}, and the actuator AB (3) is also connected rigidly at an adjustable angle λ_{34} to the flap on B. The revolute joint A connects the two actuators. The two piezo-actuators have a free curvature f. The flap moves due to the actuators' bending as the curvature radius decreases. At first, the actuators bend under the flaps weight (see Fig. 2). The horizontal starting position is adjusted by the counterweight's position on the flap's shaft.
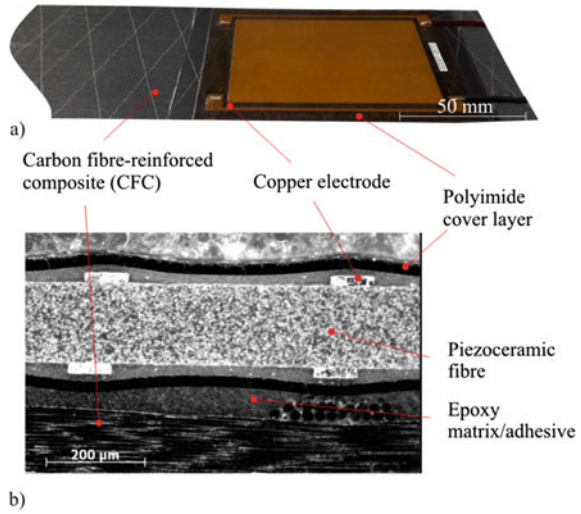
The first zone of the actuator is composed of a carbon fiber-reinforced composite (CFC) passive layer 0.25 mm thick. In the second actuator zone, on the CFC layer is bonded a 0.28 mm thick macro fiber composite (MFC) actuator layer.

3   Equivalent Two-Layered Pseudo Rigid Body Active Model Cell

The active element presented in Fig. 3 consists of a passive base layer and an actuator layer. The base layer function is to enable a large non-linear elastic deformation of the flexible active element and a large strain without damage initiation.

By the inverse piezoelectric effect used for actuation, the strain S depends on the load T and the electric field strength E. Considering the tensor of mechanical parameters on the crystal surface, the vector linear equation in Voigt's notation is:

Fig. 3 Illustration of an
active element

a)

Carbon fibre-reinforced
composite (CFC)   Copper electrode

Polyimide
cover layer

Piezoceramic
fibre

Epoxy
matrix/adhesive

b)

$$\{S\} = \left[s^E\right] \cdot \{T\} + \left[d^t\right] \cdot \{E\} \tag{1}$$

where $[d^t]$ is the matrix for the reverse piezoelectric effect and $[s^E]$ the compliance
matrix for E = 0.

The two-layer cells simulation model (Mărgineanu 2014) for an ACM ensuring
both compliance and an actuation is composed of a six-bar linkage as in Fig. 4. The
passive layer is simulated by the rocker 6 $A_{p,j-1}A_{p,j}$ with the length L_0. The total
deformation x_4 of the active layer 2, 3, 4, $A_{a,j-1}A_{a,j}$ rotates the interface link 5
around the revolute joint $A_{p,j}$ simulating the actuator's bending.

The bending compliance of the passive layer was simulated by torsion
spring-dampers inserted in the revolute joints $A_{p,j}$. As two springs were connected
on each side of the interface element to ensure equal angles with the current and the
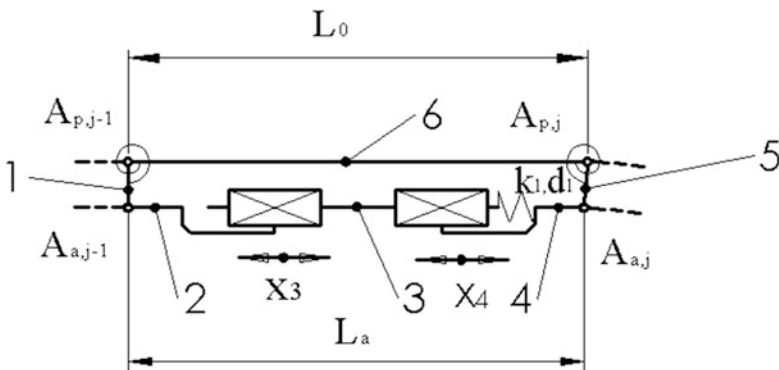
Fig. 4 Representation of a modelling cell

previous layer elements, the rigidity of these springs was double compared to the equivalent bending rigidity of the passive layer:

$$k_\theta = \frac{2M_j}{\theta} = 2E_p \cdot \frac{I_z}{L_0} = E_p \cdot \frac{B_p \cdot H_p^3}{6L_0} \tag{2}$$

with B_p, the width and H_p, the thickness of the passive layer, and the damping:

$$d_\theta = D_p \cdot \frac{B_p \cdot H_p^3}{6} \cdot \sqrt{E_p \cdot \rho_p} \tag{3}$$

where D_p is the damping grade, E_p is the Young's modulus, ρ_p is the density, and B_p, the width and H_p the thickness of the passive layer.

The deformation x_3 in the active prismatic joint under pulsating input Voltage signal with the amplitude U_{amp} and the frequency ω_e is:

$$x_3(t) = \frac{d_{33} \cdot U_{amp} \cdot L_0}{2 \cdot t_{IDE}} \cdot (1 - \cos(\omega_e \cdot t)) \tag{4}$$

where d_{33} is the piezoelectric constant and $t_{IDE,}$ the distance between electrodes.

The elastic deformation of the actuator layer under load is simulated by the spring-damper with the rigidity k_l:

$$k_l = E_a \cdot \frac{B_a \cdot H_a}{L_0} \tag{5}$$

and the damping coefficient:

$$d_l = 2D_a \cdot B_a \cdot H_a \cdot \sqrt{E_a \cdot \rho_a} \tag{6}$$

where D_a is the damping grade, E_a is the Young's modulus and ρ_a is the density of the piezoceramic's element's material, and B_a, the width and H_a the thickness of the active layer.

4 Analytic Dynamics Study of an Actuating Layer

The dynamic model for the active layer is shown in Fig. 5. The link 5 guides the exciter 3 moving with $x_3(t)$ according to Eq. 4. The driven link's 4 movement law $x_4(t)$ is determined by the dynamic equilibrium equation of forces acting on it:

$$\overrightarrow{F_i(t)} + \overrightarrow{F_d(t)} + \overrightarrow{F_{el}(t)} = \overrightarrow{F_{ext}(t)} \tag{7}$$
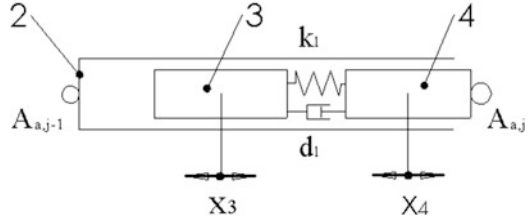
where $F_i(t)$ is the inertial force:

$$F_i(t) = -m_{red} \cdot \ddot{x}_4 \qquad (8)$$

with m_{red}, the ACM reduced mass on the cell's tip, $F_d(t)$ is the damping force:

$$F_d(t) = -d_l \cdot (\dot{x}_4 - \dot{x}_3) \qquad (9)$$

and $F_{el}(t)$ is the spring force:

$$F_{el}(t) = -k_l \cdot (x_4 - x_3) \qquad (10)$$

The differential equation may be written in scalar form, by substituting $x_3(t)$ as:

$$m_{red} \cdot \ddot{x}_4 + d_l \cdot \dot{x}_4 + k_l \cdot x_4 = \frac{k_l \cdot A_a}{2} - \frac{A_a}{2} \cdot (k_l \cos(\omega_e t) + \omega_e d_l \sin(\omega_e t)) + F_{ext}(t) \qquad (11)$$

with the actuation amplitude A_a:

$$A_a = \frac{d_{33} \cdot U_{amp} \cdot L_0}{t_{IDE}} \qquad (12)$$

The Eq. 11 shows that the piezo-actuation with a pulsating input Voltage signal is equivalent to an actuation with a step signal and an harmonic signal, both half excitation amplitude high.

Dividing by the reduced mass, the Eq. 11 becomes:

$$\ddot{x}_4 + 2\delta_l \omega_0 \dot{x}_4 + \omega_0^2 x_4 = \frac{\omega_0^2 A_a}{2} + \frac{\omega_0^2 A_a}{2} \left(2 \frac{\omega_e}{\omega_0} \delta_l \sin(\omega_e t) - \cos(\omega_e t) \right) + \frac{F_{ext}(t)}{m_{red}} \qquad (13)$$

where

$$\omega_o = \sqrt{\frac{k_l}{m_{red}}} \qquad (14)$$

$$\delta_l = \frac{d_l}{2\sqrt{k_l m_{red}}} \tag{15}$$

is the natural frequency and the damping ratio of the system.

The solution for the Eq. 13 is obtained by adding the solutions of three linear differential equations, corresponding to constant force excitation, periodic excitation, and external load, respectively:

$$\ddot{x}_4 + 2\delta_l\omega_0\dot{x}_4 + \omega_0^2 x_4 = \frac{\omega_0^2 A_a}{2} \tag{16}$$

$$\ddot{x}_4 + 2\delta_l\omega_0\dot{x}_4 + \omega_0^2 x_4 = \frac{\omega_0^2 A_a}{2\cos(\phi)}\sin(\omega_e t - \phi) \tag{17}$$

where the excitation phase angle is:

$$\phi = \arctan\left(2\frac{\omega_e}{\omega_0}\delta_l\right) \tag{18}$$

$$\ddot{x}_4 + 2\delta_l\omega_0\dot{x}_4 + \omega_0^2 x_4 = \frac{F_{ext}(t)}{m_{red}} \tag{19}$$

The solutions for the Eqs. 16 and 17 are (Dresig 2014), for an under-damped system as is the case for most ACM, respectively:

$$x_{41}(t) = \frac{A_a}{2}(1 - e^{-\delta_l\omega_0 t})\sin\left(\sqrt{1 - \delta_l^2}\,\omega_0 t\right) \tag{20}$$

$$x_{42}(t) = \frac{A_a}{2\omega_e\sqrt{\left((2\omega_0\delta_l)^2 + \left(\frac{\omega_0^2}{\omega_e^2} - 1\right)^2\right)}}\sin\left(\sqrt{1 - \delta_l^2}\,\omega_0 t + \varphi\right) \tag{21}$$

The solution for the Eq. 19 depends on the external loads, and is difficult to be obtained analytically. For this, a dynamic Multi Body System (MBS) analysis using SolidWorks Motion was performed and is presented in the following part of the manuscript.

5 Dynamic Simulation of a Multi Body System

A simplified CAD model for the ACM (see Fig. 6) is used for the simulation. A wide bending actuator was used instead of the two narrow ones. All the passive elements which were not influencing the system's dynamic behaviour (axes,
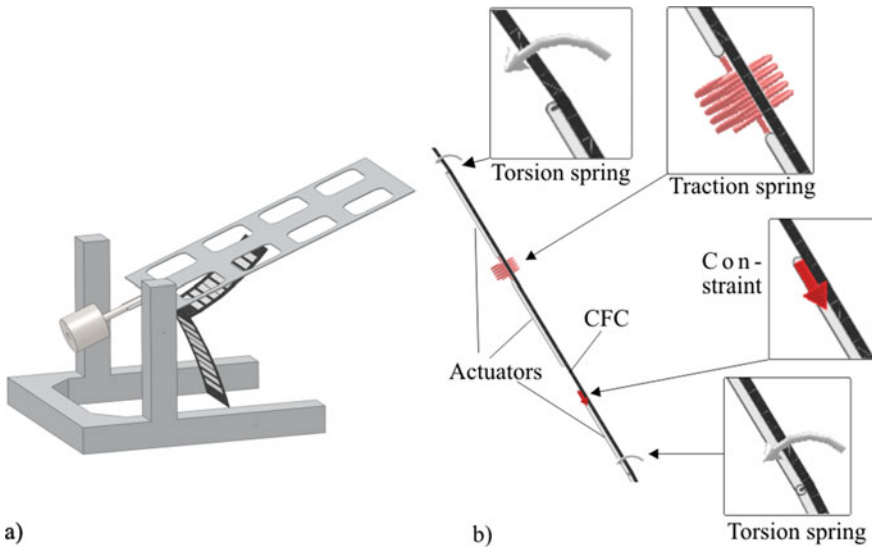
Fig. 6 ACM-Modell: **a** CAD model used for simulations; **b** simulation cell

bearings, housings, fixtures, bumpers, spacers, etc.) were substituted with constraints.

Using the simulation cell in Fig. 4, the bending actuators were simulated in the initial position with an angle constraint between the passive layers of the two subsequent simulating cells.

The simulating cell with two layers is shown in Fig. 6, with traction springs in red, torsion springs in grey and actuating movement shown by a red arrow. The revolute joints were simulated by coaxial constraints, and the prismatic joints, by co planarity constraints. The simulation parameters, calculated according to the Eq. 2–6 with the values given in Table 1 are summarized in Table 2.

Table 1 Dimensions and densities of the simulation elements for bending actuators

Parameter/element j	Thickness H [mm]		Length Lj [mm]	Width B [mm]		Density ρ [kg/m³]	
1, 5, 6, 10,	0.25		13.5	75		1750	
2, 3, 4, 7, 8, 9	H_p	H_a	29	B_p	B_a	ρ_p	ρ_a
	0.25	0.28		75	57	1750	4750

Table 2 Simulation parameters for the equivalent spring dampers and linear motors

Torsion spring damper in the passive layer		Traction spring damper in the active layer		Linear motor
Rigidity [N mm/°]	Damping coefficient [N mm/(°/s)]	Rigidity [N/mm]	Damping coefficient [N/(mm/s)]	Stroke [mm]
2	1	16,700	100	0.02

The flap's movement was recorded as the relative angular displacement in the coaxial constraint simulating the revolute joint B_0. The data were exported and were used for the comparison with the experimental results.

6 Experimental Investigation on an ACM Demonstrator

The demonstrator ACM was tested with similar parameters as used in simulations and measured with acceptable accuracy by an optical contactless dynamic 3D analysis system PONTOS (type 5 M, GOM mbH), which avoids any mechanical influence of measuring forces on the ACM. The experimental setup for both actuating and the measuring devices are shown in Fig. 7.

The input voltage for the compliant piezoactuators was provided by a high voltage power amplifier (type PA05039, smart materials GmbH) controlled by an adapted LabVIEW program used to generate various inputs with adjustable amplitude, frequency and number of cycles. A pulsating 5 or 10 cycles with the frequencies of 0.5, 1, 2 and 5 Hz input signal from 0 to 750 V was applied to the MFC.
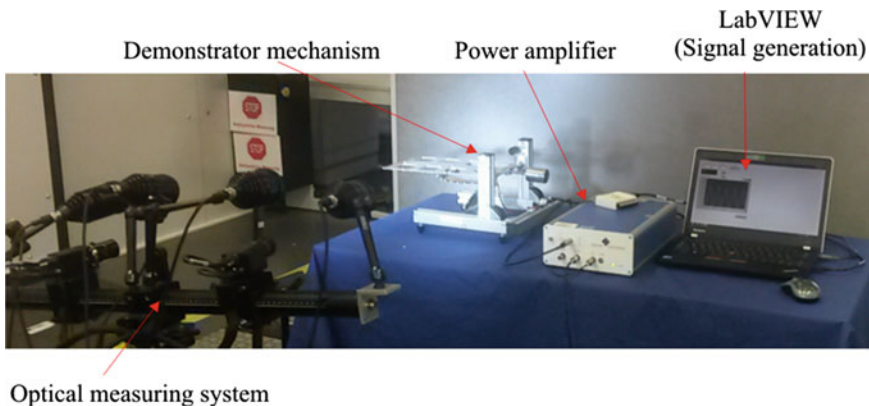
Fig. 7 Experimental set-up of the ACM demonstrator

# 7 Comparison Between Simulation and Experimental Results

A comparison between simulation and experimental results is presented in Fig. 8 up to Fig. 11.

For the overcritical case, above 1 Hz input excitation signal, the flap opened 10 degrees up. Then it oscillated around that position with $\pm 4°$ in simulation and $\pm 2°$ in experiment, as it is shown in Fig. 9. The phase difference was also obvious between the input signal and the excited oscillation.

At a higher 2 Hz frequency, shown in Fig. 10, the excited oscillation was visible also in the rising stage, accompanied by a free lower (0.75 Hz) frequency oscillation at the first 4 to 5 cycles. The oscillation amplitude decreased to $\pm 1.5°$ in simulation and $\pm 0.5°$ in experiment.

In Fig. 11, at 5 Hz, the excited oscillation was less visible, both at simulation and experiment, as predicted by Eq. 21, as the free oscillation were clearly noticeable.

After the end of excitation, the flap dropped and oscillated freely around the horizontal position. At all frequencies, the hysteresis effect was visible in tests, as the flap did not regained its horizontal position, as by the purely mechanical dynamic simulation.
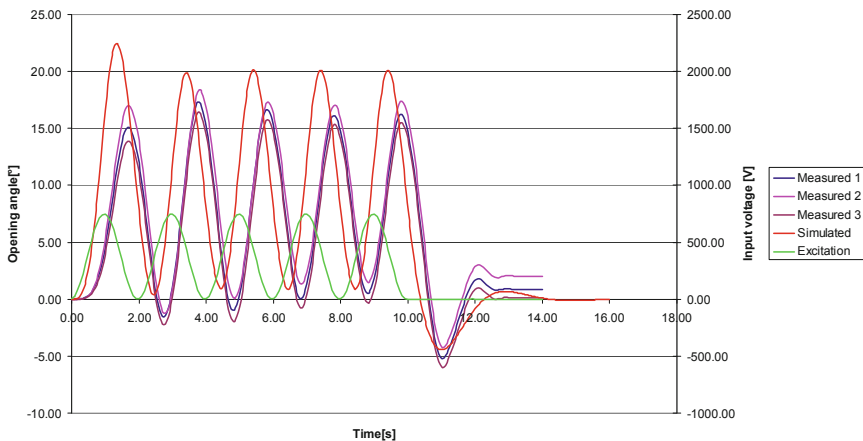
Fig. 8 Simulation and experimental results for an input voltage of 750 V at 0.5 Hz
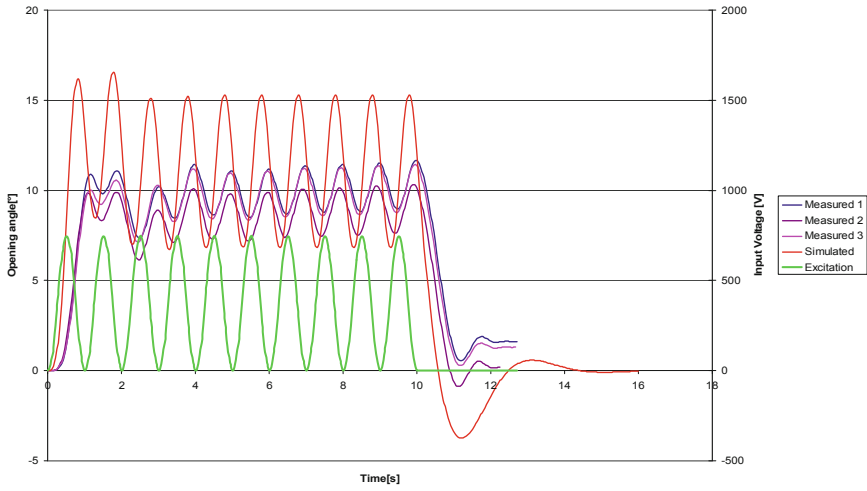
Fig. 9 Simulation and experimental results for an input voltage of 750 V at 1 Hz
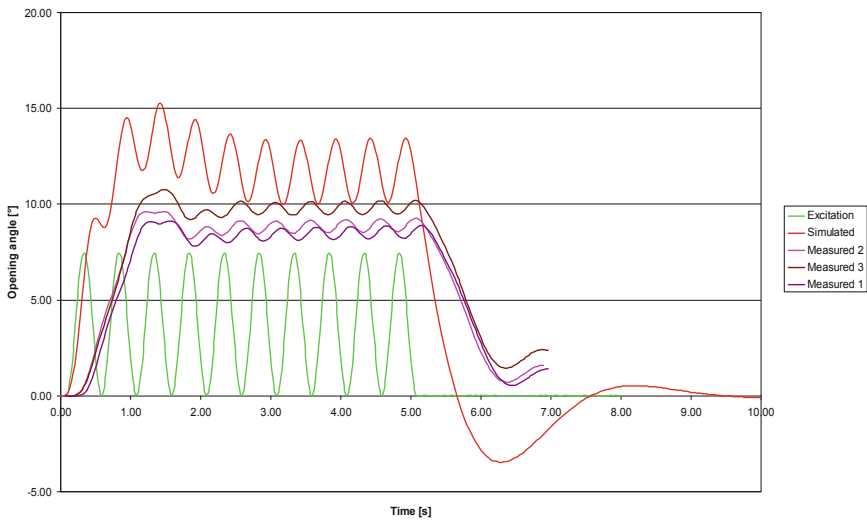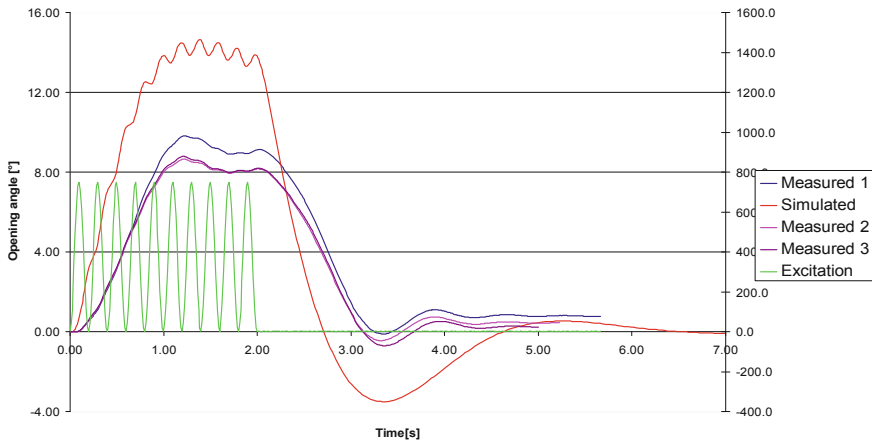

Fig. 10 Simulation and experimental results for an input voltage of 750 V at 2 Hz

Fig. 11 Simulation and experimental results for an input voltage of 750 V at 10 Hz

8   Conclusions

An under-damped piezo-driven ACM demonstrator showed a particular behavior by over-critical pulsating excitation, i.e. adding a displacement like excited with a step signal half amplitude high and a harmonic oscillation with lower amplitude, both in simulation and in experiment. This could be verified also by the proposed dynamic model of the piezo-driving layer.

The observed scatter of the experimental results between different measurements at the ACM demonstrator revealed the need to further improve and tune the developed experimental set-up. However, the scientific goal here was to investigate the dynamic behavior of an active compliant mechanism with integrated piezoceramic actuators by under- and overcritical periodic excitation. Therefore the here presented experimental set-up was considered a valid basis for this purpose, and an improvement is already planned.

In general, a good accordance between simulation and experimental results was confirmed. The existing discrepancies can be explained due to the assumed simplifications taken into account at the simulation model. The temperature effects and the frequency-dependent material properties that could further deviate the results, were not taken into consideration. In future investigations the occurring damping effects and the required damping coefficients must be further modeled and a new comparison must be undertaken.

References

Dresig H, Fidlin A (2014) Schwingungen und mechanische Antriebssysteme: modellbildung, Berechnung, Analyse, Synthese. 3. Auflage. Springer Vieweg Verlag

Gao ZH, Zhang, D (2010) Design, analysis and fabrication of a multidimensional acceleration sensor based on fully decoupled compliant parallel mechanism. Sens Actuators A 163

Mărgineanu D et al (2014) Multibody system simulation of hysteresis effect by micro textile-reinforced compliant mechanisms with piezo-electric actuators, MAMM Timişoara

Modler N (2008) Nachgiebigkeitsmechanismen aus Textilverbunden mit integrierten aktorischen Elementen. Dissertation Technische Universität Dresden

Modler N et al (2009) A design of compliant mechanisms with integrated actuators. SYROM - Braşov (Romania), pp 655–664

Tanık E, Söylemez E (2010) Analysis and design of a compliant variable stroke mechanism. Mech Mach Theory 45:1385–1394